121.9-Gb/s PDM-OFDM Transmission With 2-b/s/Hz Spectral Efficiency Over 1000 km of SSMF

Sander Lars Jansen, *Member, IEEE*, Itsuro Morita, Tim C. W. Schenk, *Member, IEEE*, and Hideaki Tanaka

***Abstract*—We discuss optical multi-band orthogonal frequency division multiplexing (OFDM) and show that by using multiple parallel OFDM bands, the required bandwidth of the digital-to-analogue/ analogue-to-digital converters and the required cyclic prefix can significantly be reduced. With the help of four OFDM bands and polarization division multiplexing (PDM) we report continuously detectable transmission of 10×121.9-Gb/s (112.6-Gb/s without OFDM overhead) at 50-GHz channel spacing over 1,000-km standard single mode fiber (SSMF) without any inline dispersion compensation. In this experiment 8 QAM subcarrier modulation is used which confines the spectrum of the 121.9 Gb/s PDM-OFDM signal within a 22.8 GHz optical bandwidth. Moreover, we propose a digital signal processing method to reduce the matching requirements for the wideband transmitter IQ mixer structures required for PDM-OFDM.**

***Index Terms*—Chromatic dispersion compensation, fiber-optic transmission systems, long-haul transmission, orthogonal frequency-division multiplexing (OFDM).**

I. Introduction

OPTICAL networks are currently shifting towards a data-centric configuration, in which the transport of internet protocol (IP) traffic is expected to play a more dominant role. 100 Gigabit Ethernet (100 GbE) is considered to become the next generation Ethernet standard for IP networks [1]. Consequently, research has recently accelerated into finding appropriate long-haul Ethernet transport solutions for the physical layer [2]–[4]. In the short term, multi-wavelength transport might provide a solution for 100-Gb/s Ethernet, but in the long run a single-wavelength solution will be the most cost-effective approach.

Different modulation formats such as on-off keying (OOK) and differential quadrature phase-shift-keying (DQPSK) have been proposed for the realization of 100 GbE. On a 100-GHz grid, 107-Gb/s vestigial sideband (VSB) OOK transmission has been realized over 510 km [2], 107-Gb/s NRZ-DQPSK over 1,200 km [3], and 100-Gb/s DQPSK-modulated coherent-WDM over 1,300 km [4]. However, in these experiments direct detection is employed, resulting in a limited chromatic dispersion (CD) and polarization mode dispersion (PMD) tolerance. This can be alleviated through optical compensation, but this is not suitable for cost-sensitive applications. The tolerance towards these linear impairments can be increased significantly through the use of coherent detection. In combination with digital signal processing, coherent receivers can provide a superior tolerance towards chromatic dispersion and PMD [5], [6]. Recently several high data rate experiments have been reported, showing a large dispersion and PMD tolerance [7]–[11].

Although all of these experiments employ a coherent receiver, they can be differentiated into systems that use either blind channel estimation [7]–[9] or training symbol (TS) based channel estimation [10], [11]. Typically, systems with blind estimation employ few subcarriers (1 to 4) whereas systems using training symbol have many subcarriers (more than 50). A well known modulation format that uses blind channel estimation is polarization-division-multiplexed QPSK (PDM-QPSK). Blind channel estimation requires a careful design of the channel estimation algorithm so that the system converges under all conditions. Especially in links with high CD and PMD this in not trivial. When training symbols are used, channel estimation becomes straightforward which has proved to significantly simplify scaling to higher level modulation formats [10], [12]. However, the main disadvantage of TS-based channel estimation is that the overhead is increased by about 8% for an optimally designed system [10]. A more detailed comparison between blind and TS-based channel estimation is reported in [13]. Note that all systems that employ orthogonal subcarriers are often referred to as orthogonal frequency division multiplexed (OFDM) system, independent of whether blind [9] or TS-based [10], [11] channel estimation is used.

In this paper, we focus on OFDM as a digital multicarrier technique using TS-based channel estimation. We elaborate on [10] and discuss in more detail the transmission experiment of 121.9-Gb/s (112.6-Gb/s without OFDM overhead) PDM-OFDM over 1,000 km of fiber. Furthermore, we look into transmitter IQ imbalance compensation and propose an algorithm to compensate for frequency selective IQ imbalance, which can significantly relax the requirements (and thereby cost) of the IQ mixers at the transmitter.

The paper is structured as follows. In Section II the principle and implications of multi-band OFDM is explained for 100 GbE PDM-OFDM. Subsequently, the experimental setup and results of the 121-Gb/s PDM OFDM experiment are described in Sections III and IV, respectively. Then Section V provides

Manuscript received July 15, 2008; revised October 03, 2008. Current version published February 13, 2009. This work was supported in part by a project of the National Institute of Information and Communications Technology of Japan.

S. L. Jansen was with KDDI R&D Laboratories, Saitama, 356-8502 Japan. He is now with Nokia Siemens Networks, 81827 Munich (e-mail: Sander.Jansen@nsn.com).

I. Morita and H. Tanaka are with KDDI R&D Laboratories, Saitama, 3568502 Japan (e-mail: Morita@kddilabs.jp; hide@kddilabs.jp).

T. C. W. Schenk is with Philips Research, Eindhoven, 5656 AE The Netherlands (e-mail: Tim.Schenk@philips.com).

Color versions of one or more of the figures in this paper are available online at http://ieeexplore.ieee.org.

Digital Object Identifier 10.1109/JLT.2008.2007972

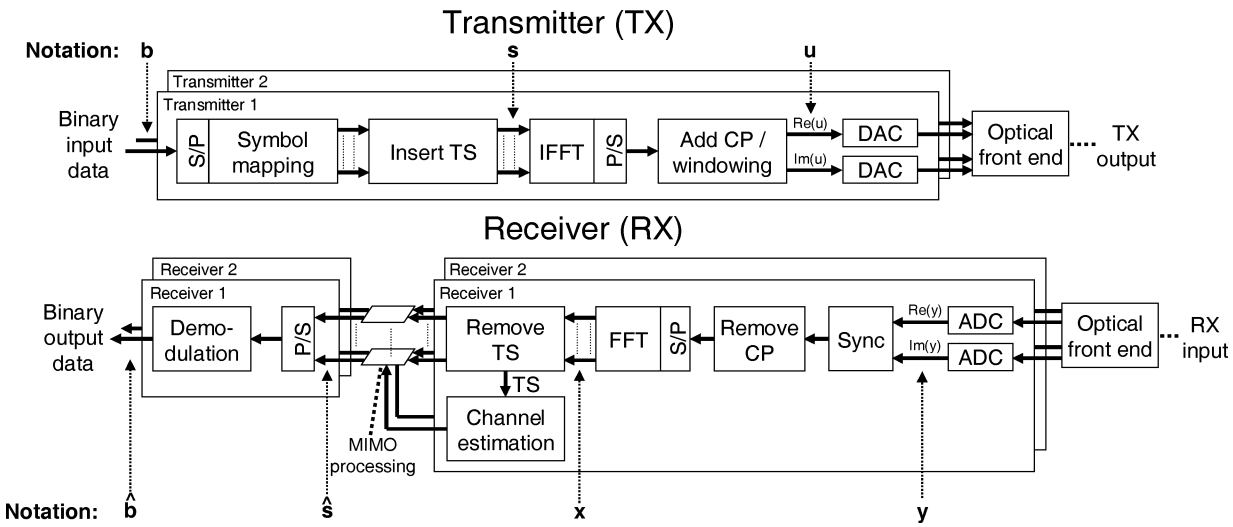

Fig. 1. Block diagram of a typical PDM-OFDM transmitter and receiver detailing the baseband processing, with CP = cyclic prefix, TS = training symbol, Sync. = Symbol Synchronization, SFO = sample frequency offset, P = parallel and S = serial.

an approach and algorithm for the compensation of frequency selective IQ imbalance and finally in Section VI we draw the conclusions.

II. PDM-OFDM Transceiver Design

In this section we treat different aspects and considerations for the design and implementation of the PDM-OFDM systems. First we briefly discuss the baseband generation and detection of a PDM-OFDM signal. Subsequently, different options for the optical front end are considered.

A. Baseband PDM-OFDM

Fig. 1 illustrates the block diagram of a PDM-OFDM transmitter and receiver. For simplicity, a perfectly synchronized system is assumed in this illustration, meaning that the carrier frequency offset (CFO) [14] and local oscillator phase noise [15] is compensated for. The notation vectors shown in Fig. 1 consist of two elements, one for each transmitter, defined for data stream $\mathbf{b} = [b_1 \quad b_2]^{\mathrm{T}}$, where the index denotes the number of the transmitter and $^{\mathrm{T}}$ denotes the transpose operation. Note that in the following vectors and matrices are denoted by bold lower and upper case symbols, respectively.

The binary data stream $\mathbf{b}$ is converted from serial to parallel and symbol mapping is applied. Periodically, training symbols (TS) are then inserted resulting in the complex signal vector $\mathbf{s}$. Subsequently, the signal is modulated onto orthogonal carriers by applying the inverse fast Fourier transform (IFFT). After the IFFT, a cyclic prefix (CP) is added to mitigate impairments caused by for instance chromatic dispersion or PMD, yielding the OFDM baseband vector $\mathbf{u}$. Windowing is applied to reduce the out-of-band power of the OFDM signal. When both negative and positive subcarriers are modulated, $\mathbf{u}$ is a complex vector, so that the baseband signal of each transmitter must first be split into a real and an imaginary part before they are converted to analogue signals using digital-to-analogue converters (DACs). The optical front end thus receives two signals per transmitter, i.e., the real and imaginary part, that are subsequently combined by an IQ mixer, which in Fig. 1 is part of the optical front end.

At the receiver, the outputs of the optical front end are first digitized using analogue-to-digital converters (ADCs), yielding vector $\mathbf{y}$. After the ADCs, symbol synchronization is applied as described in [14], [16], [17]. Both transmitters operate at the same symbol rate, so the symbol timing needs only to be recovered for one of the transmit streams. After removing the CP, the OFDM signal is converted back to the frequency domain by applying the FFT, yielding signal vector $\mathbf{x}$. Then the training symbols are removed from the payload and used for channel estimation. Subsequently, MIMO processing per subcarrier is applied to de-rotate the polarization of the received symbols, yielding estimated signal vector $\hat{\mathbf{s}}$. Finally, these symbols are demodulated (or demapped) resulting in vector $\hat{\mathbf{b}}$, containing the estimates of the transmitted data. For more details on the MIMO processing the reader is referred to [6], [18].

B. Optical Front End

One of the main challenges for high speed fiber-optic OFDM systems is probably the realization of the DACs and ADCs that are required at the transmitter and receiver, respectively. In [15] we have shown that the required bandwidth for both DACs and ADCs can be relaxed by using multiple subcarrier multiplexed OFDM bands. Multi-band OFDM modulation is a common technique in wireless applications and in fiber-optic OFDM transmission systems this concept is often referred to as subcarrier multiplexing (SCM) [15], [19]. In this section the advantages and disadvantages of multi-band OFDM will be discussed and compared with single-band OFDM for a 100-GbE OFDM signal with PDM.

1) Single-Band OFDM: Although 100 GbE has not been standardized yet, it is foreseen that 7% overhead needs to be allocated for forward error correction (FEC) and about 4% for the Ethernet protocol (64 B/66 B coding). This results in a raw data rate of 111 Gb/s. In an OFDM signal additional overheads are caused by the cyclic prefix, the training symbols and the pilot subcarriers for phase noise compensation. Especially for high data rates it is essential to minimize the OFDM related overhead as it significantly increases the bandwidth requirements at

the transmitter and receiver. In [15] we showed that by using an RF-pilot tone, phase noise compensation can be realized without pilot subcarriers and as such the total OFDM overhead can be reduced to about 8% (see [10] or the discussion section in [6]). All overheads combined (7% FEC, 4% protocol and 8% OFDM related), the required nominal data rate for a 100 GbE OFDM system is at least 120 Gb/s. The bandwidth of a PDM-OFDM signal, denoted as B_{d} [Hz], can be expressed as

$$B_{\mathrm{d}} = \frac{R_{\mathrm{nominal}}}{2 \cdot \log_2(M)} \tag{1}$$

where R_{nominal} is the nominal data rate [b/s], M is the constellation size, i.e., the number of data-points per subcarrier per OFDM symbol, and the factor 2 results from the use of PDM. The bandwidth of a 120-Gb/s PDM-OFDM signal with QPSK modulation of the subcarriers is thus 30 GHz. The cyclic prefix required for the mitigation of chromatic dispersion is dependent on the bandwidth of the OFDM signal and the desired transmission distance [15]. A good estimate for the required guard time τ_{g} is

$$\tau_{\mathrm{g}} = D \cdot B_{\mathrm{d}} \cdot \frac{c}{f^2} \tag{2}$$

where D represents the chromatic dispersion of the desired transmission distance [s/m], B_{d} is the effective bandwidth of the modulated OFDM signal as defined in (1), c is the speed of light [m/s] and f represents the center frequency of the OFDM band [Hz]. For a 1000-km link of SSMF with 16-ps/nm/km chromatic dispersion a minimal cyclic-prefix guard band of $\tau_{\mathrm{g}} = 3.9$ ns/OFDM symbol is required in this configuration. The fast Fourier transform (FFT) of the OFDM system must now be chosen such that the cyclic prefix and training symbol overhead do not exceed the initial estimated 8% OFDM overhead allocated in the nominal data rate. Assuming 6.7% oversampling at the transmitter the sampling rate of the DAC is 32 GHz. It is now easily shown that an FFT size of 4096 is needed so that the OFDM symbol duration is $4096/32 \cdot 10^9 = 128$ ns excluding cyclic prefix (131.9 ns including cyclic prefix). With this configuration, the overhead for cyclic prefix is about 3.5% [15], leaving 4.3% overhead for training symbols. Oversampling at the transmitter is required to spectrally separate the aliasing products that are generated by the DAC from the OFDM signal so that the aliasing products can be removed with a low-pass filter. The 6.7% oversampling, as assumed in this example, provides a 1-GHz guard band between the aliasing products and the OFDM signal which is more than sufficient for most low-pass filters [15].

Several methods exist to modulate an OFDM signal onto an optical carrier. For the complex-valued OFDM signals that are most commonly used in systems with coherent detection [10], [11] in-phase (I) and quadrature (Q) mixing is required at the transmitter and at the receiver. This IQ mixing can either be realized in the electrical [10] or the optical domain [11].

A possible transmitter implementation for the electrical and optical IQ mixer are illustrated in Fig. 2. Note that the generation of only one polarization of the PDM signal is shown throughout

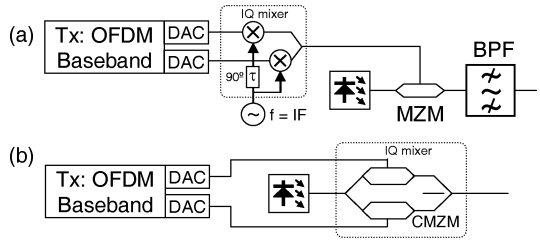

Fig. 2. Single band OFDM transmitters, based on an (a) electrical IQ mixer (b) optical IQ mixer.

this section. At the transmitter the OFDM signal is generated in the digital domain and the real and imaginary part of the OFDM signal are converted to the analogue domain by two DACs. In order to suppress aliasing components at the output of a DAC or the input of an ADC, a LPF is required. Because these LPF filters are used for every DAC or ADC, they are for simplicity not shown in the transmitter and receiver configurations discussed in this section. After the LPFs, the signal is fed to the IQ multiplexer. When an electrical IQ mixer is used the signal is upconverted to an intermediate frequency, which is typically slightly higher than half of the bandwidth of the OFDM signal. A conventional single-ended MZM (Mach-Zehnder modulator) is then used for the modulation of the OFDM signal onto the optical carrier. Apart from the modulated OFDM signal, this modulator creates an image band as well, mirrored with respect to the carrier frequency (f_{c}). A BPF [15] or interleaver [6] must therefore be used to remove the imageband after modulation. An elegant method to avoid the generation of the image band is by using an optical IQ mixer. A common implementation of an optical IQ mixer/modulator is a complex Mach–Zehnder modulator (CMZM), with two parallel MZMs within a super Mach–Zehnder structure. In order to realize the IQ mixing, the relative phase shift between the two parallel modulators is $\pi/2$. With such an optical IQ mixer, the OFDM signal is directly modulated onto the optical signal without imageband and thus no optical filtering is required at the transmitter.

Similar to the transmitter, the receiver can be realized with either electrical [Fig. 3(a)] or optical IQ mixing [Fig. 3(b)]. In the receiver configuration with an electrical IQ mixer the LO is placed next to the OFDM signal so that after coherent detection with a 180 degrees optical hybrid an intermediate frequency is present in the detected OFDM signal. This receiver configuration is commonly referred to as a superheterodyne or heterodyne receiver. With the 180 degrees optical hybrid only one side of the LO spectrum is detected and as such an optical BPF is required at the input of this detector to suppress image noise. The output of the hybrid is detected with a photodiode and the signal is then downconverted into the baseband by an electrical IQ mixer and converted to the digital domain with two ADCs. Alternatively, an optical IQ mixer can be used to directly downconvert the OFDM signal into the baseband. In the fiber-optic community this detection method is commonly referred to as homodyne or intradyne detection, in the wireless community this method is also known as direct downconversion. The LO is for this method placed in the middle of the OFDM signal and

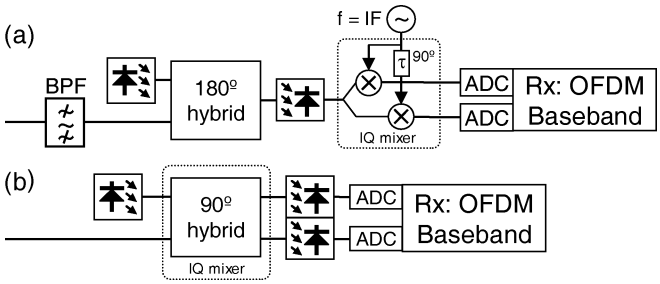

Fig. 3. Single-band OFDM receivers, based on an (a) electrical IQ mixer and (b) optical IQ mixer.

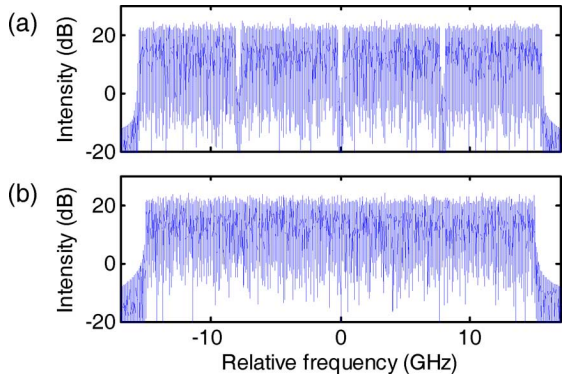

Fig. 4. Simulated optical spectra of 120-Gb/s PDM-OFDM with (a) four OFDM bands and (b) a single OFDM band.

a 90 degrees optical hybrid is used as optical IQ mixer. The 90 degrees hybrid outputs the real and imaginary part of the down-converted signal that are subsequently detected by two photodiodes and converted into the digital domain with two ADCs.

Under ideal conditions, the performance of the two transmitter and receiver structures is the same and any combination of transmitter and receiver structure can be used. Note that in Fig. 3, the receivers are shown with single ended photodiodes. Alternatively balanced photodiodes could be used to cancel unwanted mixing products of the subcarriers end of neighboring WDM channels. However, under optimal operating conditions these unwanted mixing products are small and thus no significant performance increase can be obtained by using balanced photodiodes.

In the configuration shown in Fig. 2(a) the OFDM signal is upconverted to an intermediate frequency before modulation, which increases the bandwidth requirements of the optical modulator by about a factor of two. However, for the 120-Gb/s PDM-OFDM signal, the required electrical bandwidth for the single ended MZM would be approximately 30 to 40 GHz, which is currently commercially available. The bandwidth requirements of the modulator and detector configurations for the DAC and ADC requirements are exactly the same. For the 120-Gb/s PDM-OFDM signal, discussed in the previous section, the DACs and ADCs require 15 GHz of bandwidth with a sampling rate of at least 32 GHz (Assuming 6.7% oversampling).

2) Multi-Band OFDM: Fig. 4 shows the spectrum of a multi-band 100 GbE PDM-OFDM signal. In this particular example four individual bands are used with QPSK modulation per subcarrier. For a fair comparison with the single-band OFDM system the same number of modulated subcarriers is used, resulting in an FFT-size of 1024 per OFDM band. As a consequence of this configuration, the overhead with respect to training symbols is identical to that of the single-band OFDM system. The PDM-OFDM signal consists in this case of four OFDM bands that are each 7.5-GHz wide. The reduction of the width of the OFDM bands has some implications on the configuration and the performance of the system. According to (2), the minimum required guard time in this case is about 1 ns/OFDM symbol instead of the 3.9 ns/OFDM symbol required for the single band configuration. This results in a reduction of the cyclic prefix overhead with a factor of four to less than 1%. Another consequence of reducing the OFDM band is that the guard band between the aliasing products and the OFDM signal becomes smaller for the same oversampling rate. In order to maintain the 1-GHz oversampling guard band, the oversampling ratio must be increased to 26.7%. This increase in oversampling increases the OFDM symbol rate as well. As a result, the symbol length is slightly reduced to $1024/9.5 \cdot 10^9 = 108$ ns excluding cyclic prefix and 109 ns including cyclic prefix.

The change in FFT-size of 4096 to 4×1024 has some implications on the DSP complexity of the system as well. This complexity is often expressed in the number of complex multiplications per second. For an N-point FFT, $(N/2)\log_2(N)$ complex multiplications are required [20]. In the multi-band OFDM configuration four FFTs of 1024 each must be taken per OFDM symbol at transmitter and receiver, resulting in 40,960 computations per OFDM symbol per polarization. This corresponds to $3.79 \cdot 10^{11}$ complex multiplications per second. In the single-band OFDM case one 4096 FFT at both TX and RX is performed per OFDM symbol resulting in 49,152 complex multiplications, which corresponds to $3.65 \cdot 10^{11}$ complex multiplications per second. Thus, by splitting the single-band OFDM signal into individually modulated OFDM bands, the computational complexity remains practically the same. Apart from the FFT processing, there is also little difference between the digital signal processing complexity of single and multi-band OFDM in the rest of the system (channel estimation, mapping, etc) because the total number of modulated subcarriers is the same.

In principle multi-band OFDM can be generated in the digital domain. Modulation and detection can then be realized the same way as single band OFDM (e.g., Figs. 2 and 3). This is a very straightforward approach that requires the least discrete components for its realization. However, it requires the same electrical bandwidth of the DACs and ADCs as in single band modulation. Furthermore, additional complex multiplications are required to downconvert all OFDM bands in the electrical domain, making the difference in complexity compared to single band OFDM almost zero. By generating and detecting the OFDM bands independently, the DAC requirements for multi-band OFDM can significantly be relaxed. In this case the multiplexing and demultiplexing of the OFDM bands is realized in the analogue domain.

Three transmitter configurations for combining four OFDM bands in the analogue domain are shown in Fig. 5. When IQ mixing is realized with electrical mixers only at the transmitter,

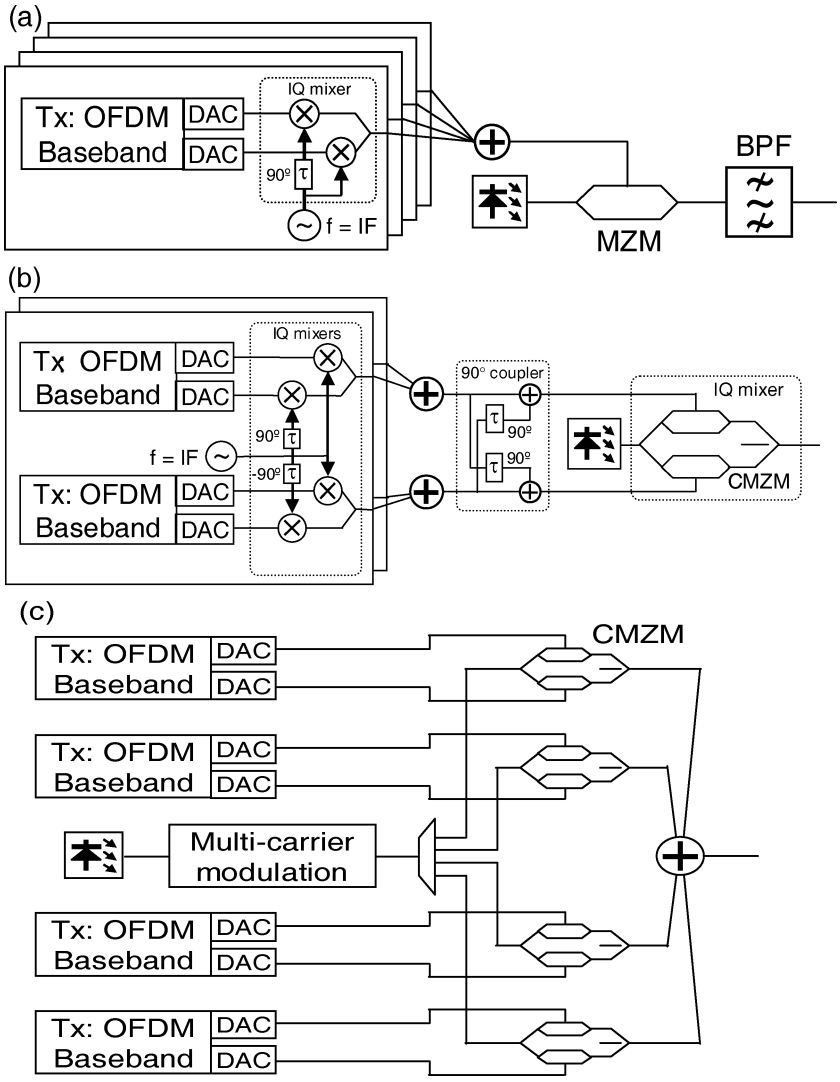

Fig. 5. Multi-band OFDM transmitters, based on (a) electrical IQ mixers, (b) hybrid electrical and optical IQ mixers, and (c) optical IQ mixers.

four IQ-mixers are used at four different intermediate frequencies. Subsequently these four OFDM bands are combined and a conventional single-ended MZM is used for modulation. Similar to the single-band modulator structure with an electrical IQ mixer, an optical filter is used after modulation to remove the imageband that is created by the single-ended MZM.

The number of intermediate frequencies can be reduced by a factor of two by using a CMZM instead of a conventional single-ended MZM. In this case, two times two bands are multiplexed in the electrical domain with 90 degrees difference in phase for orthogonality. Then these bands are combined with a 4-port 90-degrees directive coupler [21] (basically applying the Hilbert transform) and modulated onto an optical carrier with a CMZM. The four OFDM bands can in this configuration be created by IQ-multiplexing in both the electrical and the optical domain. First the four OFDM basebands are upconverted to two different intermediate frequencies. Subsequently, these two OFDM bands are once again IQ modulated with an optical IQ mixer. As no image band is generated with the optical IQ mixer no BPF is needed at the output. Another advantage of this technique is that only half the intermediate frequencies are required which lowers the required modulator bandwidth by a factor of two. The main disadvantage of the hybrid electrical and optical IQ mixer approach is that for each OFDM band two IQ mixers are used, namely one to upconvert the baseband onto an IF and one to modulate the optical carrier. As such, this setup is impaired by two sorts of implementation imperfections concerning the IQ matching: The conventional IQ mismatch between the real and imaginary part of the baseband transceiver, i.e., the IQ imbalance induced by the electrical IQ mixer, and that of the CMZM, i.e., the optical IQ mixer.

Finally one can realize the IQ mixing completely in the optical domain. In this case each OFDM band is modulated onto an optical carrier with an optical IQ-mixer individually. The optical carriers are generated by multi-carrier modulating a CW laser and splitting the subcarriers with an optical filter [22]. Recently an integrated modulator has been reported that would be capably of modulating two individual OFDM bands [9].

Three receiver configurations for demultiplexing a four-band OFDM signal in the analogue domain are illustrated in Fig. 6, providing the reverse operation of the transmitter structures in Fig. 5. The configurations shown in Fig. 6(a) and (b) are basi-

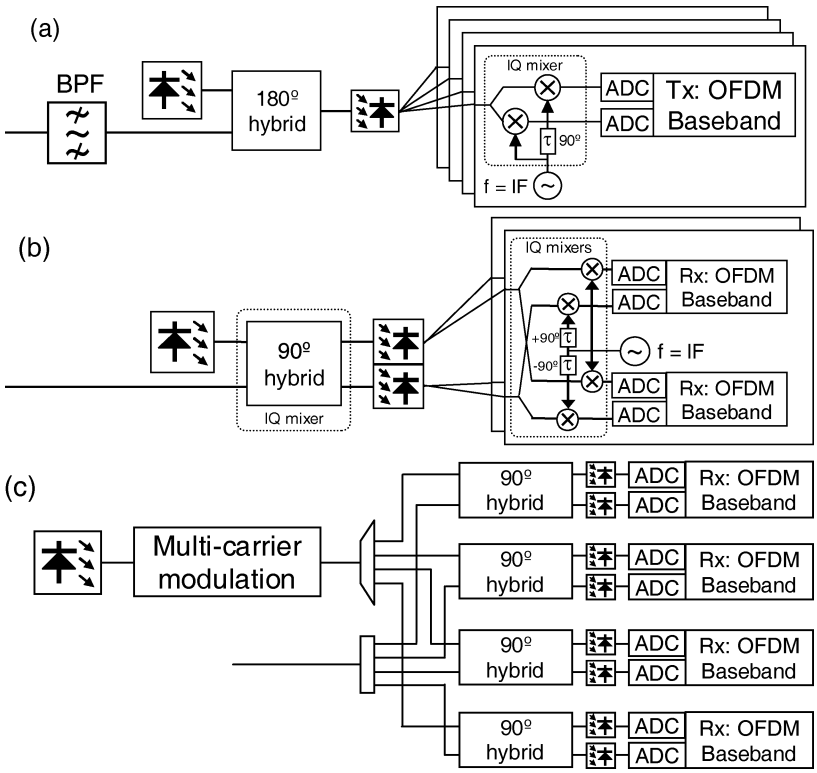

Fig. 6. Multi-band OFDM receivers, based on (a) electrical IQ mixers, (b) hybrid electrical and optical IQ mixers, and (c) optical IQ mixers.

cally the multi-channel approaches of the single carrier receivers shown in Fig. 3(a) and (b), respectively. Here the optical hybrid is used to down convert all the OFDM bands at the same time with one 180 or 90 degrees hybrid. Subsequently, the intermediate frequency (IF) signal is further downconverted by the electrical IQ mixers or balanced mixers for the configuration shown in Fig. 6(a) and (b), respectively. Note that similar to the single band coherent receivers an optical BPF is required at the input of the 180 degrees hybrid in order to suppress image noise.

Fig. 6(c) shows a per-band receiver based on optical IQ mixers only. Basically this receiver consists of a 90° hybrid receiver per OFDM band. For each of these receivers a LO is required. A possibility for providing the LO would be to use an individual laser per OFDM band. A more practical approach might be to use a multi-carrier modulator similar as that of the transmitter to create the LO wavelengths for all bands with one single laser. This not only reduces the cost and power consumption, the received OFDM bands now have the same phase noise as well as they are produced by the same laser, which enables the use of one single phase noise compensation scheme for all OFDM bands.

Compared to single-band OFDM, the DAC/ADC requirements of multi-band are reduced by the number of bands used. In the case of 120-Gb/s PDM-OFDM with four OFDM bands, the bandwidth of each OFDM band is 7.5 GHz instead of 30 GHz. As a result, the required DAC/ADC bandwidth is only 3.75 GHz with a sampling rate of at least 9 GHz. The downside is that for all configurations that use analogue OFDM-band mixing two DAC-ADC pairs are required for each OFDM band, resulting in a total of sixteen pairs for the generation and detection of the 100 GbE PDM-OFDM signal (8 pairs per polarization). It can thus be concluded that the use of multi-band OFDM greatly simplifies the complexity in the digital domain, but at the cost of an increased complexity in the analogue domain. A potential method to reduce the cost of multi-band OFDM is by applying electric and or photonic integration [23].

Note that in the multi-band spectrum shown in Fig. 4 a small guard band is present between the OFDM bands. This guard band can be eliminated by using a coherent source for the OFDM bands [11], [22] and subsequently setting the intermediate frequency between the OFDM bands to exactly a multiple of the symbol rate. Furthermore, the symbol rate and phase of the individual OFDM bands must be precisely synchronized. Coherent modulation of the OFDM bands makes most sense for systems with a low number of subcarriers (100 and less) as for these systems the out of band crosstalk is the largest [11], [22]. For OFDM systems with a high number of subcarriers, the out of band crosstalk is that low that the OFDM bands can be packed tightly together [10] so that coherent modulation would make little difference and would unnecessarily increase system complexity.

III. Experimental Setup

In this section we show the principle of multi-band OFDM using the multiplexing scheme with electrical IQ mixers as shown in Fig. 5(a). At the receiver, a broadband 90° hybrid is used as shown in Fig. 3(b). After coherent detection, the individual OFDM bands are downconverted in the digital domain, resulting effectively in the receiver configuration shown in Fig. 6(b) with ideal IQ mixers.

The experimental configuration for the 100 GbE multi-band PDM-OFDM setup is shown in Fig. 7. In this experiment,

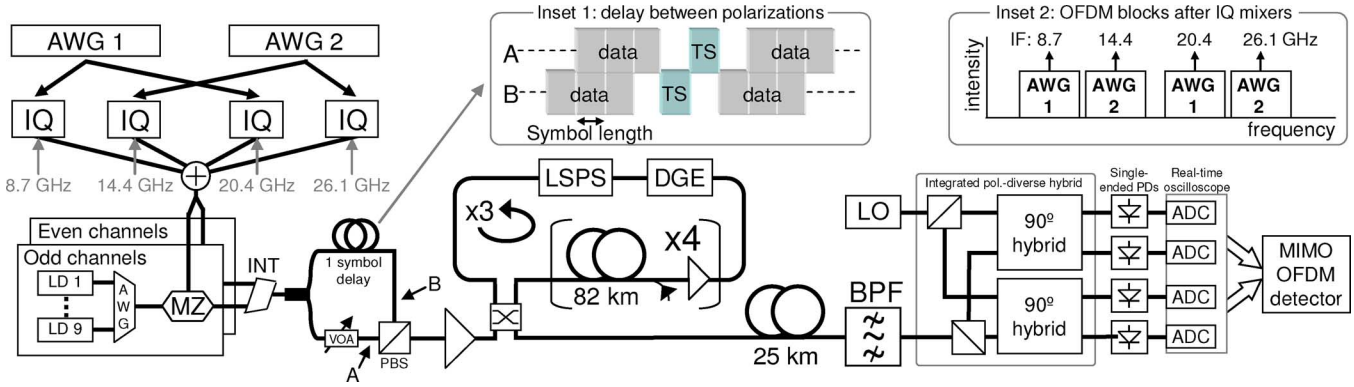

Fig. 7. Experimental setup, with IQ = inphase-quadrature mixer, LD = laser diode, INT = 50-GHz interleaver, TS = training symbol, LSPS = loop-synchronous polarization scrambler, DGE = dynamic gain equalizer, ADC = analogue-to-digital converter.

Tektronix AWG7102 arbitrary waveform generators (AWG) are used at a sampling rate of 10 GSamples/s to emulate the generation of the OFDM basebands. The baseband waveforms that are produced by the AWGs have been calculated offline and are outputted continuously. The OFDM signal consists of two polarization-multiplexed signals with four multi-band OFDM bands each. The 121.9-Gb/s signal has therefore a total of eight 15.2-Gb/s tributaries. In order to create this multi-band signal, the two OFDM baseband signals are upconverted to four IFs, present at 8.7 GHz, 14.4 GHz, 20.4 GHz and 26.1 GHz. Inset 2 of Fig. 7 illustrates the electrical OFDM channel allocation after upconversion. As only two AWGs were available care was taken in this setup that neighboring OFDM bands are generated by different AWGs for decorrelation, Therefore, AWG 1 is used for the first (8.7 GHz) and third OFDM (20.4 GHz) bands and AWG 2 for the second (14.4 GHz) and fourth (26.1 GHz).

The FFT size is 1024, from which 520 subcarriers are effectively used for the transport of data. As discussed in Section II-B2, the minimal required cyclic prefix for this configuration in a 1000-km link is about 1 ns. In this experiment a larger cyclic prefix of 22 samples (2.2 ns) per OFDM symbol was chosen to relax the synchronization requirements at the receiver after transmission. Together with the cyclic prefix, the OFDM symbol length is 104.6 ns and the OFDM symbol rate 9.6 MHz. This symbol length is slightly shorter than that discussed in Section II-B2, namely 104.6 ns instead of 109 ns, because the oversampling used was slightly higher. A non-rectangular 8-QAM constellation is used for symbol mapping, which provides the maximum symbol distance and consequently the best bit-error rate (BER) versus signal-to-noise ratio (SNR) performance [24], [25]. For some specific subcarriers, the electrical SNR was not sufficient to support 8-QAM modulation. The SNR at these subcarriers are impaired by for instance side-modes of the local oscillator laser or frequency selective IQ imbalance of the electrical IQ-mixers. Therefore, 5% extra OFDM channels had to be allocated at the transmitter which are omitted at the receiver. In a practical system one could signal this back to the transmitter and transmit the data on these subcarriers using a lower constellation size, such as QPSK or BPSK, and only the carriers with the worst SNR empty. This is known as adaptive modulation and is used extensively in radio and cable communications [30], e.g., in WiMax and DSL. Such an adaptive modulation technique would allow for an increased data rate. However, in this experiment this was not possible as each AWG was driving two IQ mixers at different intermediate frequencies. More details about the OFDM baseband generation and IQ-mixing can be found in [15]. For this WDM experiment, 10 external cavity lasers (ECLs) with an approximate linewidth of 100 kHz are aligned on a 50-GHz ITU grid between 1553.7 nm and 1557.4 nm. Two parallel Mach–Zehnder modulators are used in this setup for separate modulation of the even and odd channels. The optical modulators are single-ended Mach–Zehnder modulators designed for analog applications (Avanex AM-40). In order to suppress the carrier of the OFDM signal the modulator is biased in its minimum. After modulation, the even and odd WDM channels are combined using a 50 GHz interleaver. As described in [6] the interleaver is aligned such that the image band of the OFDM signal is rejected. Polarization multiplexing is emulated by splitting the signal with a 3-dB coupler and combining it with a polarization beam combiner. As shown in inset 1 of Fig. 7, one arm is delayed by exactly one OFDM symbol (104.6 ns) for decorrelation. The bit rate before coding is 121.9 Gb/s, from which 6% is used for training symbols and 2.15% for the cyclic prefix. Before FEC this results in a data rate of 112.6 Gb/s allowing transport of Ethernet frames with 7% FEC and up to 4% protocol overhead. Fig. 3(a) shows the optical spectrum of the 121.9-Gb/s OFDM signal, which clearly indicates the well defined optical spectrum with a 22.8 GHz bandwidth.

The re-circulating loop consists of 4 spans of 82-km SSMF without optical dispersion compensation. After every span, amplification is provided by a Raman/EDFA structure with an average on/off Raman gain of $\sim$ 10 dB. A dynamic gain equalizer (DGE) is used for power equalization and a loop-synchronous polarization scrambler (LSPS) is employed to reduce loop-induced polarization effects. After transmission, 25 km of SSMF is inserted, resulting in a total transmission distance of 1,009 km. At the receiver, the signal is split in two random polarizations and is detected with a polarization-diverse 90 degrees optical hybrid. An ECL with $\sim$ 100-kHz linewidth is used as free running local oscillator (LO) and four single-ended 20-GHz Pin/TIA modules (Discovery DSC-R401HG) are used for detection. A real-time digital storage oscilloscope (Tek-

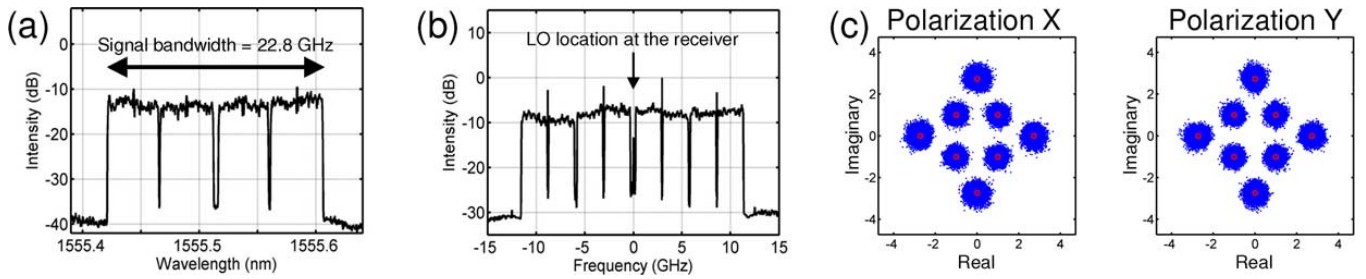

Fig. 8. (a) Measured optical spectrum of the 121.9-Gb/s PDM OFDM (100-MHz res bw). (b) Calculated electrical spectrum after coherent detection (20-MHz res bw). (c) Scatterplot of the 1st OFDM band of the 121.9-Gb/s PDM OFDM signal (all subcarriers).

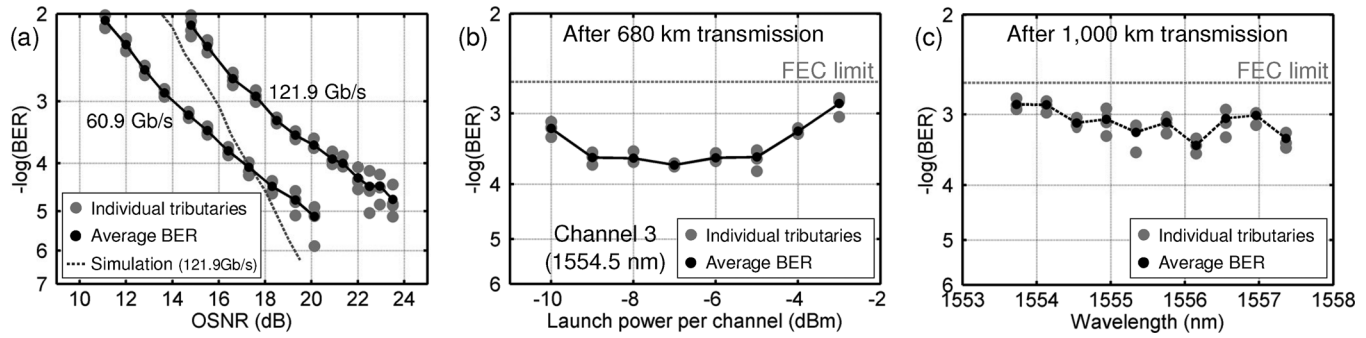

Fig. 9. (a) B2B sensitivity. (b) Power excursion after 680-km transmission. (c) BER after 1000-km transmission.

tronix DPO72004) is used to sample the four outputs of the optical hybrid. The bandwidth of the oscilloscope is 16 GHz, the sampling frequency is 50 GHz and the effective number of bits is approximately 5.5 bits. After detection, the data is post-processed off-line. Fig. 8(b) shows the computed electrical spectrum after coherent detection. The LO is located in the middle of the OFDM signal, in between the second and third OFDM bands.

Training symbols are periodically inserted into the OFDM signal, so that polarization de-rotation at the receiver can be realized through MIMO processing. The processing algorithm is described in detail in [6]. In order to distinguish between the training symbols of the PDM tributaries the training symbols should be received one after the other. The delay of the PDM emulator is exactly one OFDM symbol, thus training is realized in this experiment by inserting an empty OFDM symbol before and after the training symbol (see inset 1 of Fig. 7). Because of the empty OFDM symbol that is inserted for every training period, the training period consists in the experiment of three symbols instead of two. As a result, the overhead caused by training symbols can be reduced from 6% by 4% when the two polarizations are modulated independently (see for instance [6]) instead of the PDM emulator that is used in this experiment.

In order to compensate for the phase noise of the local oscillator, RF-aided phase noise compensation is implemented (for the implementation, see [15]). In order to mitigate the influence of amplified spontaneous emission (ASE) noise on the channel estimation, a moving average over 12 training symbols was used for MIMO processing at the receiver. For all reported BER results five sets with each 2.4 million bits have been evaluated, each set with different polarization state settings in the LSPS.

IV. Experimental Results

Fig. 9(a) shows the measured back-to-back sensitivities for 60.9 Gb/s (single polarization) and 121.9 Gb/s (PDM). Additionally, the simulated sensitivity for 121.9 Gb/s is shown as well. The required optical signal-to-noise ratio (OSNR) for a BER of 1×10^{-3} is 14 dB/0.1 nm and 17.8 dB/0.1 nm for 60.9 Gb/s and 121.9 Gb/s, respectively. Apart from the 3-dB expected penalty, a 0.8-dB excess penalty is observed for PDM. This penalty is most likely caused by a less effective phase noise compensation scheme. Because of the one symbol delay in the PDM emulator at the transmitter, there is a 105-ns delay between the RF-pilot tones of the two polarizations. At the receiver, the sum of these RF-pilot tones is used for phase noise compensation and thus the delay between the polarizations reduces the effectiveness of the phase noise compensation scheme. We note that this penalty only applies for our emulated PDM setup and that in a convention PDM setup with a modulator per polarization such a penalty has not been observed [6]. Compared to the simulated sensitivity of 121.9 Gb/s, a penalty of about 2 dB at a BER of 1×10^{-3} is present. For lower BER values an increase in performance penalty between the simulated and experimental curve is observed. This penalty increase is most likely caused by the fact that at lower BER values the residual carrier frequency offset and phase noise after compensation start influencing the system performance [18]. Additionally, the performance of the fourth OFDM band is limited by nonlinearities of the amplifiers and frequency mixer. As a result, a BER floor is observed for this OFDM band, limiting the BER of the 121.9-Gb/s configuration to about 5×10^{-6}.

The fiber launch power optimization for channel 3 (located at 1554.5 nm) after 680-km transmission is shown in Fig. 9(b). The BER performance shows little variation over a wide launch power range (from -9 dBm to -5 dBm). At higher fiber launch powers a steep increase in BER is observed due to the influence of nonlinearities. For a similar PDM-OFDM transmission experiment on the same fiber type it has been observed in [6] that even at a 50-GHz channel spacing, SPM is dominant over inter-channel nonlinear impairments (XPM and FWM). The nonlinear tolerance could be increased by reducing the constellation size to QPSK, however, this would require a larger electrical bandwidth (which was not available for this experiment). Fig. 9(c) shows the performance of the 10 WDM channels after 1.000-km transmission (with -7 dBm/channel launch power). The average OSNR after transmission is $\sim$ 21.5 dB and the average BER per channel varies between 3.9×10^{-4} and 1.3×10^{-3}. Compared to the back-to-back performance, a BER penalty of about one decade is observed after transmission due to residual nonlinear impairments. The channels on the red side of the spectrum slightly outperform the other channels as the noise figure of the EDFA/Raman amplifiers is slightly lower for these wavelengths, which results in a $\sim$ 0.4-dB higher OSNR. The obtained BER values are well below the threshold of a concatenated FEC code with 7% overhead (2.3×10^{-3}).

V. IQ Imbalance Compensation

The transmitter and receiver of the 121.9-Gb/s PDM OFDM setup, described in this manuscript are realized with discrete components. In this setup, the matching of the I and Q ports of the IQ mixers showed to be a key parameter in the design of the transmitter. Because of the AWG and lowpass filters used before the IQ-mixers, a frequency selective behavior in this IQ imbalance is observed for all four OFDM bands. In this setup electrical delay lines were used for each IQ mixer to minimize the average time delay between the I and Q channel and the frequency selective IQ imbalance was minimized by using high quality lowpass filters. A more cost-effective approach would be to compensate for the IQ imbalance in the digital domain at the receiver. Such compensation techniques are receiving an increased interest for wideband wireless systems, as it significantly reduces the requirements of the IQ mixers and thereby the system complexity and cost. Typically the bandwidth of the OFDM signals in wireless applications is relatively small (typically below 50 MHz) and consequently for these systems the IQ imbalance is usually constant over the whole OFDM band. It is thus not surprising that most proposed IQ imbalance compensation schemes in wireless applications do not take frequency selective IQ imbalance into account (see for instance [26] and [27]). As the data rate of fiber-optic OFDM systems is significantly higher than that used in wireless systems the OFDM bands are larger and more susceptible to frequency selective IQ imbalance.

Some algorithms have been proposed for the suppression of frequency selective IQ imbalance influence in the receiver. In [31] an adaptive filter based approach is proposed for the compensation of imbalance between the low-pass filters in the receiver. Moreover, an (offline) calibration-based compensation solution for frequency selective receiver IQ imbalance is treated in [28]. In contrast, for the setup considered in this work, it was found that the dominant source of IQ imbalance is in the transmitter. It is therefore noted that calibration based compensation of transmitter induced frequency selective IQ imbalance is significantly harder than for receiver IQ imbalance. This would typically require an additional and perfectly matched calibration receiver to be added to the transmitter, to allow for accurate compensation. Therefore, we propose to compensate for the influence of the transmitter IQ mismatch in the receiver of the communication system, since it does not require additional hardware.

In this section we expand on the TX frequency independent IQ imbalance compensation algorithm proposed in [18] and show how to realize the TX frequency selective IQ imbalance compensation in the receiver by employing a specifically designed set of training symbols. This approach is selected above an adaptive filter based approach, since it achieves convergence much faster.

The PDM-OFDM system illustrated in Fig. 1 can effectively be described as a 2×2 MIMO system. For a system without IQ imbalance the signal model for the received kth subcarrier can be written as

$$\mathbf{x}(k)=\mathbf{H}(k)\mathbf{s}(k)+\mathbf{n}(k), \tag{3}$$

where $\mathbf{x}(\mathrm{k})=[\,x_1(\mathrm{k})\quad x_2(\mathrm{k})\,]^{\mathrm{T}}$ and $\mathbf{s}(\mathrm{k})=[\,s_1(\mathrm{k})\quad s_2(\mathrm{k})\,]^{\mathrm{T}}$. The receiver noise vector and channel matrix for the kth subcarrier are denoted by $\mathbf{n}(\mathrm{k})=[\,n_1(\mathrm{k})\quad n_2(\mathrm{k})]^{\mathrm{T}}$ and

$$\mathbf{H}(k)=\begin{bmatrix}H_{11}(k) & H_{12}(k)\\ H_{21}(k) & H_{22}(k)\end{bmatrix} \tag{4}$$

respectively. An estimate of the transmitted signal vector can subsequently be found using MIMO processing. Different algorithms have been proposed for this in literature for MIMO wireless communications, see e.g., [29] for an overview. Here we focus on the most straight-forward MIMO processing know as zero-forcing (ZF) processing. The ZF detection yields

$$\hat{\mathbf{s}}(k)=\mathbf{H}^{+}(k)\mathbf{x}(k)=\mathbf{s}(k)+\mathbf{H}^{+}(k)\mathbf{n}(k) \tag{5}$$

where $^{+}$ denotes the pseudo-inverse operation, defined for a matrix $\mathbf{A}$ as $\mathbf{A}^{+}=(\mathbf{A}^{\mathrm{H}}\mathbf{A})^{-1}\mathbf{A}^{\mathrm{H}}$. Here $^{\mathrm{H}}$ and $^{-1}$ denote the conjugate transpose and matrix inverse, respectively.

Subsequently, we consider a system which is impaired by frequency selective IQ imbalance at the transmitter, due to imperfect matching between the I and Q branch. The resulting baseband equivalent time-domain transmit signal can be written as

$$\begin{aligned}\widetilde{\mathbf{u}}(t)&=\mathbf{f}_{\mathrm{I}}(t)*\Re\{\mathbf{u}(t)\}+j\mathbf{f}_{\mathrm{Q}}(t)*\Im\{\mathbf{u}(t)\}\\&=\frac{\mathbf{f}_{\mathrm{I}}(t)+\mathbf{f}_{\mathrm{Q}}(t)}{2}*\mathbf{u}(t)+\frac{\mathbf{f}_{\mathrm{I}}(t)-\mathbf{f}_{\mathrm{Q}}(t)}{2}*\mathbf{u}^{*}(t)\end{aligned} \tag{6}$$

where $\mathbf{f}_{\mathrm{I}}$ and $\mathbf{f}_{\mathrm{Q}}$ denote the impulse responses of the I and Q branch, $\Re\{\mathbf{u}(\mathrm{t})\}$ and $\Im\{\mathbf{u}(\mathrm{t})\}$ denote the real and imaginary part of $\mathbf{u}(\mathrm{t})$, * denotes convolution and $\mathbf{u}^{*}(\mathrm{t})$ denotes the complex conjugate of $\mathbf{u}(\mathrm{t})$.

In the frequency domain this results in

$$\widetilde{\mathbf{s}}(k)=\frac{\mathbf{F}_{\mathrm{I}}(k)+\mathbf{F}_{\mathrm{Q}}(k)}{2}\mathbf{s}(k)+\frac{\mathbf{F}_{\mathrm{I}}(k)-\mathbf{F}_{\mathrm{Q}}(k)}{2}\mathbf{s}^{*}(-k) \tag{7}$$

where $\mathbf{F}_{\mathrm{Q}}(k)$ and $\mathbf{F}_{\mathrm{I}}(k)$ are 2×2 diagonal matrices, which are the frequency response for both polarization channels of the I and Q branch, respectively. Carriers left and right from the DC carrier are assigned a negative and positive carrier index, respectively. Hence, carrier k and $-k$ have the same distance from the DC carrier and are consequently often referred to as mirror carriers. We can observe from (7) that the IQ mismatch results in a leakage of the signal component of carrier $-k$ into that of carrier k and vice versa. Note that when there is perfect matching between the I and Q branch, i.e., $\mathbf{F}_{\mathrm{I}}(k)=\mathbf{F}_{\mathrm{Q}}(k)$, the second term in (7) reduces to 0 and there is no leakage.

The above yields the following expression for the received signal for the kth subcarrier:

$$\widetilde{\mathbf{x}}(k)=\mathbf{H}(k)\widetilde{\mathbf{s}}(k)=\mathbf{H}(k)\frac{\mathbf{F}_{\mathrm{I}}(k)+\mathbf{F}_{\mathrm{Q}}(k)}{2}\mathbf{s}(k)+\mathbf{H}(k)\frac{\mathbf{F}_{\mathrm{I}}(k)-\mathbf{F}_{\mathrm{Q}}(k)}{2}\mathbf{s}^{*}(-k). \quad (8)$$

Note that for simplicity we omitted the influence of noise in this expression.

When we now combine the signal model for carrier k and $-k$, we get the 4×1 vector $\mathbf{x}(k,-k)$ given by

$$\begin{aligned}&\begin{bmatrix}\widetilde{\mathbf{x}}(k)\\ \widetilde{\mathbf{x}}^{*}(-k)\end{bmatrix}\\ &=\begin{bmatrix}\mathbf{H}(k)\frac{\mathbf{F}_{\mathrm{I}}(k)+\mathbf{F}_{\mathrm{Q}}(k)}{2} & \mathbf{H}(k)\frac{\mathbf{F}_{\mathrm{I}}(k)-\mathbf{F}_{\mathrm{Q}}(k)}{2}\\ \mathbf{H}^{*}(-k)\frac{\mathbf{F}_{\mathrm{I}}^{*}(-k)+\mathbf{F}_{\mathrm{Q}}^{*}(-k)}{2} & \mathbf{H}(-k)\frac{\mathbf{F}_{\mathrm{I}}^{*}(-k)+\mathbf{F}_{\mathrm{Q}}^{*}(-k)}{2}\end{bmatrix}\\ &\quad\times\begin{bmatrix}\mathbf{s}(k)\\ \mathbf{s}^{*}(-k)\end{bmatrix}\\ &=\begin{bmatrix}\widetilde{\mathbf{H}}_{11}(k,-k) & \widetilde{\mathbf{H}}_{12}(k,-k)\\ \widetilde{\mathbf{H}}_{21}(k,-k) & \widetilde{\mathbf{H}}_{22}(k,-k)\end{bmatrix}\mathbf{s}(k,-k)\\ &=\widetilde{\mathbf{H}}(k,-k)\mathbf{s}(k,-k).\end{aligned} \quad (9)$$

Using (9), we can rewrite the PDM-OFDM system model in (3) as

$$\mathbf{x}(k,-k)=\widetilde{\mathbf{H}}(k,-k)\mathbf{s}(k,-k)+\mathbf{n}(k,-k) \quad (10)$$

for a system with frequency selective transmitter IQ imbalance, where the 4×1 vector $\mathbf{n}(k,-k)$ is constructed similarly as $\mathbf{s}(k,-k)$.

Note from (9) that the original 2×2 MIMO problem for PDM-FDM in (3) is converted into a 4×4 MIMO problem due to the transmitter IQ imbalance. Consequently, when we derive an estimate of the new 4×4 MIMO channel matrix, i.e., $\widetilde{\mathbf{H}}(k,-k)$, we can find back the transmitted signal by applying joint ZF processing for carrier k and $-k$. This will then yield

$$\begin{aligned}\hat{\mathbf{s}}(k,-k)&=\widetilde{\mathbf{H}}^{+}(k,-k)\,\mathbf{x}(k,-k)\\ &=\mathbf{s}(k,-k)+\widetilde{\mathbf{H}}^{+}(k,-k)\,\mathbf{n}(k,-k).\end{aligned} \quad (11)$$

From (11) we can conclude that we can then successfully remove the influence of the IQ imbalance.

The estimation of $\widetilde{\mathbf{H}}(k,-k)$ is performed in a similar way as the estimation of $\mathbf{H}(k)$ in the experiment presented in Section III. In the experiment time multiplexed (orthogonal) training symbols were used, see Fig. 7, to allow estimation of the channel parameters for both polarization channels. A similar approach could be applied for the estimation of $\widetilde{\mathbf{H}}(k,-k)$, i.e., applying four time multiplexed training symbols, to allow for subsequent estimation of the channel elements for all combinations of the pair of mirror carriers ($-k$ and k) and the two polarizations.

It is more power efficient, however, to apply training symbols that occupy all timeslots. That is why these are considered here. Like the time multiplexed approach, these training symbols should exhibit orthogonality for the mirror carriers and the two polarizations. We propose to use a structure consisting of 4 consecutive OFDM symbols, for which the signals on subcarriers k and $-k$ are defined by the 4×4 matrix

$$\mathbf{S}_{\mathrm{p}}(k,-k)=\begin{bmatrix}\mathbf{s}_{\mathrm{p,t1}} & \mathbf{s}_{\mathrm{p,t2}} & \mathbf{s}_{\mathrm{p,t3}} & \mathbf{s}_{\mathrm{p,t4}}\end{bmatrix} \quad (12)$$

where $\mathbf{s}_{\mathrm{p,t1}}$ denotes the 4×1 the trainings vector during the first symbol period. We propose to use the Walsh-Hadamard matrix to construct $\mathbf{S}_{\mathrm{p}}$, which provides the required orthogonality and additionally has the advantage that all symbols have unit power. It is given by

$$\mathbf{S}_{\mathrm{p}}(k,-k)=\pm\begin{bmatrix}1 & 1 & 1 & 1\\ 1 & -1 & 1 & -1\\ 1 & 1 & -1 & -1\\ 1 & -1 & -1 & 1\end{bmatrix} \quad (13)$$

where the sign can be chosen such to minimize the overall crest factor of the training symbols. When we omit the influence of noise, the received signal corresponding to these training signals is given by the 4×4 matrix

$$\mathbf{X}_{\mathrm{p}}(k,-k)=\widetilde{\mathbf{H}}(k,-k)\mathbf{S}_{\mathrm{p}}(k,-k). \quad (14)$$

Then the least squares (LS) estimate of the 4×4 MIMO channel matrix $\widetilde{\mathbf{H}}(k,-k)$ is found by multiplying the received signal in (14) with the inverse of the trainings matrix in (13), yielding

$$\begin{aligned}\hat{\mathbf{H}}(k,-k)&=\mathbf{X}_{\mathrm{p}}(k,-k)\mathbf{S}_{\mathrm{p}}^{-1}(k,-k)\\ &=\widetilde{\mathbf{H}}(k,-k)\frac{1}{4}\mathbf{S}_{\mathrm{p}}(k,-k)\mathbf{S}_{\mathrm{p}}(k,-k)=\widetilde{\mathbf{H}}(k,-k)\end{aligned} \quad (15)$$

where the last equality is due to the orthogonality between the rows of S_{p}.

The estimate of the transmitted signal can now be found using (11), when $\widetilde{\mathbf{H}}(k,-k)$ is replaced by its LS estimate as defined in (15). This corrects simultaneously for the PDM and the frequency dependent TX imbalance, allowing for lower cost IQ mixers.

To demonstrate the effectiveness of the proposed compensation approach, we simulate the constellation diagram of a 16-QAM OFDM signal with and without frequency selective IQ imbalance. The phase α and amplitude φ response of the IQ imbalance that is imposed at the transmitter is shown in Fig. 10. These are defined as the phase and amplitude of

$$\alpha e^{j\varphi}=\frac{\mathbf{F_I}(k)-\mathbf{F_Q}(k)}{\mathbf{F_I}(k)+\mathbf{F_Q}(k)} \quad (16)$$

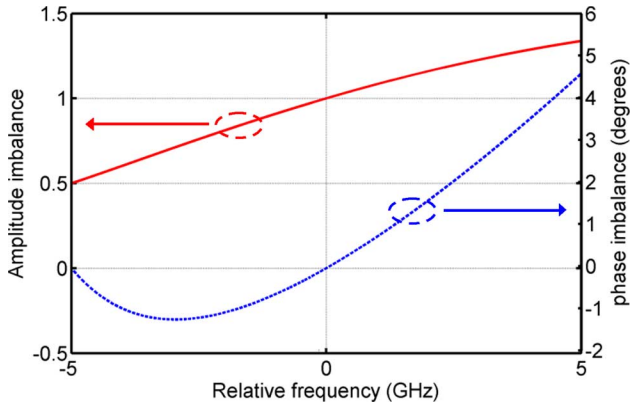

Fig. 10. Amplitude and phase response as a function of frequency for the simulated IQ imbalance.

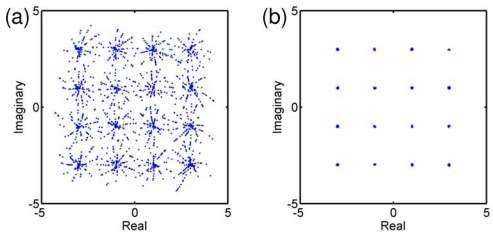

Fig. 11. Constellation diagram (overlay of all subcarriers) of a 16-QAM OFDM signal (a) without IQ imbalance compensation and (b) with IQ imbalance compensation.

respectively.

The amplitude imbalance α varies between 0.5 and 1.3 and the phase imbalance φ between $-1.2°$ and $4.6°$. Fig. 11 shows the constellation diagram of one polarization with and without IQ compensation. It can be seen that practically all IQ imbalance is compensated for.

Note that even though the influence of the mismatch in (9) was only derived for transmitter IQ imbalance, it can easily be extended to include the influence of receiver IQ imbalance as well. This will result in the same expression as in (10). Consequently, the compensation approach designed in this paper can be applied to compensate for both transmitter and receiver IQ imbalance.

VI. Conclusion

In this paper, we show that by using multiple parallel OFDM bands in an optical orthogonal frequency multiplexed (OFDM) system, the required bandwidth of the digital-to-analogue/analogue-to-digital converters and the required cyclic prefix can significantly be reduced. Using four OFDM bands, WDM transmission of 10×121.9-Gb/s polarization-division multiplexed OFDM is demonstrated at 2-b/s/Hz spectral efficiency. Transmission over 1,000 km of SSMF was achieved without any in-line chromatic dispersion compensation.

Moreover, a digital signal processing method was proposed to reduce the matching requirements for the wideband transmitter IQ mixer structures required for PDM-OFDM. The use of IQ imbalance compensation significantly relaxes the requirements at transmitter and receiver, allowing for lower cost IQ mixers.

Acknowledgment

The authors would like to thank M. Al Fiad, M. Schuster, and D. van den Borne for the many fruitful discussions and reviewing the manuscript. Furthermore, the authors thank Dr. S. Akiba and Dr. M. Suzuki for their support.

References

[1] M. Duelk, "Next-generation 100 G Ethernet," in *Proc. Eur. Conf. Opt. Commun.*, Glasgow, U.K., 2005, Tu. 3.1.2.

[2] K. Schuh, E. Lach, B. Junginger, G. Veith, J. Renaudier, G. Charlet, and P. Tran, "8 Tbit/s (80 × 107 Gbit/s) DWDM ASK-NRZ VSB transmission over 510 km NZDSF with 1 bit/s/Hz spectral efficiency," in *Proc. Eur. Conf. Opt. Commun.*, Berlin, Germany, 2007, PD 1.8.

[3] P. J. Winzer, G. Raybon, S. Chandrasekhar, C. R. Doerr, T. Kawanishi, T. Sakamoto, and K. Higuma, "10 × 107-Gb/s NRZ-DQPSK transmission at 1.0 b/s/Hz over 12 × 100 km including 6 optical routing nodes," in *Proc. Opt. Fiber Commun. Conf.*, Anaheim, CA, 2007, PDP 24.

[4] A. Sano, H. Masuda, E. Yoshida, T. Kobayashi, E. Yamada, Y. Miyamoto, F. Inuzuka, Y. Hibino, Y. Takatori, K. Hagimoto, T. Yamada, and Y. Sakamaki, "30 × 100-Gb/s all-optical OFDM transmission over 1300 km SMF with 10 ROADM nodes," in *Proc. Eur. Conf. Opt. Commun.*, Berlin, Germany, 2007, PD 1.7.

[5] H. Sun, K.-T. Wu, and K. Roberts, "Real-time measurements of a 40 Gb/s coherent system," *Opt. Exp.*, vol. 16, pp. 873–879, 2008.

[6] S. L. Jansen, I. Morita, T. C. W. Schenk, and H. Tanaka, "Long-haul transmission of 16 × 52.5-Gb/s polarization division multiplexed OFDM enabled by MIMO processing," *OSA J. Opt. Networking*, vol. 7, pp. 173–182, 2008.

[7] C. R. S. Fludger, T. Duthel, D. van den Borne, C. Schulien, E.-D. Schmidt, T. Wuth, E. de Man, G. D. Khoe, and H. de Waardt, "10 × 111 Gbit/s, 50 GHz spaced, POLMUX-RZ-DQPSK transmission over 2375 km employing coherent equalisation," in *Proc. Opt. Fiber Commun. Conf.*, 2007, PDP 22.

[8] X. Zhou, J. Yu, D. Qian, T. Wang, G. Zhang, and P. D. Magill, "8 × 114 Gb/s, 25-GHz-spaced, PolMux-RZ-8 PSK transmission over 640 km of SSMF employing digital coherent detection and EDFA-only amplification," in *Proc. Opt. Fiber Commun. Conf.*, 2008, PDP 1.

[9] E. Yamada, A. Sano, H. Masuda, T. Kobayashi, E. Yoshida, Y. Miyamoto, Y. Hibino, K. Ishihara, K. Okada, K. Hagimoto, T. Yamada, and Y. Sakamaki, "Novel no-guard-interval PDM CO-OFDM transmission in 4.1 Tb/s (50 × 88.8-Gb/s) DWDM link over 800 km SMF including 50-GHz spaced ROADM nodes," in *Proc. Opt. Fiber Commun. Conf.*, 2008, PDP 8.

[10] S. L. Jansen, I. Morita, and H. Tanaka, "10 × 121.9-Gb/s PDM-OFDM transmission with 2-b/s/Hz spectral efficiency over 1,000 km of SSMF," in *Proc. Opt. Fiber Commun. Conf.*, 2008, PDP 2.

[11] Q. Yang, Y. Ma, and W. Shieh, "107 Gb/s coherent optical OFDM reception using orthogonal band multiplexing," in *Proc. Opt. Fiber Commun. Conf.*, 2008, PDP 7.

[12] B. J. C. Schmidt, A. J. Lowery, and J. Armstrong, "Experimental demonstrations of 20 Gbit/s direct-detection optical OFDM and 12 Gbit/s with a colorless transmitter," in *Proc. Opt. Fiber Commun. Conf.*, Anaheim, CA, 2007, PDP 18.

[13] S. L. Jansen, I. Morita, K. Forozesh, S. Randel, D. van den Borne, and H. Tanaka, "Optical OFDM, a hype or is it for real?," in *Proc. Eur. Conf. Opt. Commun.*, Brussels, Belgium, 2008, Mo.3.E.3.

[14] T. M. Schmidl and D. C. Cox, "Robust frequency and timing synchronization for OFDM," *IEEE Trans. Commun.*, vol. 45, no. 7, pp. 1613–1621, Jul. 1997.

[15] S. L. Jansen, I. Morita, T. C. W. Schenk, N. Takeda, and H. Tanaka, "Coherent optical 25.8-Gb/s OFDM transmission over 4,160-km SSMF," *J. Lightw. Technol.*, vol. 26, no. 1, pp. 6–15, Jan. 2008.

[16] R. van Nee and R. Presad, *OFDM for Wireless Multimedia Communications*. Norwood, MA: Artech House, 2000.

[17] T. C. W. Schenk, M. M. de Laat, P. F. M. Smulders, and E. R. Fledderus, "Symbol timing for multiple antenna OFDM systems," in *Proc. IEEE Veh. Technol. Conf.*, 2006, vol. 3, pp. 1521–1525.

[18] T. C. W. Schenk, *RF Imperfections in High-Rate Wireless Systems*. Berlin, Germany: Springer, 2008.

[19] I. B. Djordjevic and B. Vasic, "Orthogonal frequency division multiplexing for high-speed optical transmission," *Opt. Exp.*, vol. 14, pp. 3767–3775, 2006.

[20] J. G. Proakis and D. K. Manolakis, *Digital Signal Processing: Principles, Algorithms and Applications*, 3rd ed. Englewood Cliffs, NJ: Prentice-Hall, 1995.

[21] R. Hui, "Multi-tributary OFDM optical transmitter using carrier-suppressed optical single-sideband modulation," in *Proc. Opt. Fiber Commun. Conf.*, 2003, MF74.
[22] T. Kobayashi, A. Sano, E. Yamada, H. Takara, and A. Takada, "Electro-optically subcarrier multiplexed 110 Gb/s OFDM signal transmission over 80 km SMF without dispersion compensation," in *Proc. Optoelectron. Commun. Conf.*, 2007, PD1–6.
[23] S. Corzine, P. Evans, M. Kato, G. He, M. Fisher, M. Raburn, A. Dentai, I. Lyubomirsky, R. Nagarajan, M. Missey, V. Lal, A. Chen, J. Thomson, W. Williams, P. Chavarkar, S. Nguyen, D. Lambert, T. Butrie, M. Reffle, R. Schneider, M. Ziari, C. Joyner, S. Grubb, F. Kish, and D. Welch, "10-channel $\times$ 40 Gb/s per channel DQPSK monolithically integrated InP-based transmitter PIC," in *Proc. Opt. Fiber Commun. Conf.*, Anaheim, CA, 2008, PDP 18.
[24] J. G. Proakis, *Digital Communications*. New York: McGraw-Hill, 2001.
[25] S. L. Jansen, I. Morita, and H. Tanaka, "Experimental demonstration of 23.6-Gb/s OFDM with a colorless transmitter," in *Proc. Optoelectron. Commun. Conf.*, 2007, PD1–3.
[26] M. Valkama, M. Renfors, and V. Koivunen, "Advanced methods for I/Q imbalance compensation in communication receivers," *IEEE Trans. Signal Process.*, vol. 49, 2001.
[27] T. C. W. Schenk, P. F. M. Smulders, and E. R. Fledderus, "Estimation and compensation of TX and RX IQ imbalance in OFDM-based MIMO Systems," in *Proc. IEEE Radio Wireless Symposium*, San Diego, CA, Jan. 2006, pp. 215–218.
[28] Y. Ma, W. Shieh, and Q. Yang, "Bandwidth-efficient 21.4 Gb/s coherent optical 2 $\times$ 2 MIMO OFDM transmission," in *Proc. Opt. Fiber Commun. Conf.*, 2008, JWA 59.
[29] D. Gesbert, M. Shafi, P. J. Da-shan, S. Smith, and A. Naguib, "From theory to practice: An overview of MIMO space-time coded wireless systems," *IEEE J. Sel. Areas Commun.*, vol. 21, no. 4, pp. 281–282, Apr. 2003.
[30] S. T. Chung and A. J. Goldsmith, "Degrees of freedom in adaptive modulation: A unified view," *IEEE Trans. Commun.*, vol. 49, no. 9, pp. 1561–1571, Sep. 2001.
[31] T. C. W. Schenk, P. F. M. Smulders, and E. R. Fledderus, "Estimation and compensation of frequency selective TX/RX IQ imbalance in MIMO OFDM systems," in *Proc. IEEE Int. Conf. Commun.*, Jun. 2006, vol. 1, pp. 251–256.

Sander L. Jansen (S'02–M'07) was born in Maartensdijk, The Netherlands. He received the M.Sc. and Ph.D. degrees (highest honors) in electrical engineering from the University of Technology, Eindhoven, The Netherlands. Both his master thesis and Ph.D. research were conducted at the Siemens AG in Munich, Germany. His master thesis was part of the European-funded Information Society Technologies (IST) project FASHION where he worked on ultrafast optical signal processing. The main research focus of his Ph.D. work was phase conjugation for long-haul transmission systems.

From 2006 to 2008, he was an Associate Research Engineer with KDDI R&D Laboratories, Saitama, Japan, where he specialized in OFDM for fiber-optic transmission systems. Since June 2008, he has been with Nokia Siemens Networks, Munich, Germany. He has authored and coauthored more than 70 refereed papers and conference contributions.

Dr. Jansen was awarded the IEEE Lasers & Electro-Optics Society (LEOS) Graduate Student Fellowship in 2005. Recently, he received the "KDDI 2007 Best Patent Award."

Itsuro Morita received the B.E., M.E., and Dr. Eng. degrees in electronics engineering from Tokyo Institute of Technology, Tokyo, Japan, in 1990, 1992, and 2005, respectively.

He joined Kokusai Denshin Denwa (KDD) Company Ltd. (currently KDDI Corporation), Tokyo, Japan, in 1992 and, since 1994, he has been working at their Research and Development Laboratories. He has been engaged in research on long-distance and high-speed optical communication systems. In 1998, he was on leave at Stanford University, Stanford, CA.

Tim C. W. Schenk (S'01–M'07) received the M.Sc. and Ph.D. degrees in electrical engineering from Eindhoven University of Technology (TU/e), Eindhoven, The Netherlands, in 2002 and 2006, respectively. The dissertation topic for his Ph.D. degree concerned the digital compensation of front-end impairments in multiple-antenna wireless systems.

From 2002 to 2004, he was with the Wireless Systems Research Group, Agere Systems, Nieuwegein, The Netherlands. From 2004 to 2006, he was a Research Assistant in the Radio Communications Group at TU/e. Since October 2006, he has been with Philips Research Laboratories, Eindhoven, The Netherlands, as a Senior Scientist in the Distributed Sensor Systems department His current research interests include wireless and optical communications, lighting controls, and signal processing.

Dr. Schenk was awarded the 2006 Veder Award from the Dutch Scientific Radio Fund Veder for the work related to his Ph.D. dissertation.

Hideaki Tanaka was born in Osaka, Japan, on April 5, 1961. He received the B.E., M.E., and Ph.D. degrees in electronics engineering from Osaka University, Osaka, Japan, in 1984, 1986, and 1997, respectively.

In 1986, he joined Kokusai Denshin Denwa (KDD) R&D Laboratories (currently KDDI R&D Laboratories), Tokyo, Japan. Since 1986, he has been engaged in research on high-speed semiconductor modulators, their integrated devices and design of optical submarine cable systems, optical access technologies, and Generalized Multi-Protocol Label Switching (GMPLS) technologies. Currently, he is the Senior Manager with the Optical Network Architecture Laboratory, KDDI R&D Laboratories, Inc., Saitama, Japan.

Dr. Tanaka received the Best Paper Award from Opto-Electronics Conference (OEC) in 1988, the Young Engineering Award from Institute of Electronics, Information, and Communication Engineers (IEICE) in 1993 and the Distinguished Paper Award from IEICE in 1995.